İSTANBUL TİCARET ÜNİVERSİTESİ
FEN BİLİMLERİ DERGİSİ

İstanbul Commerce University Journal of Science

http://dergipark.org.tr/ticaretfbd

Research Article / Araştırma Makalesi

EFFECT OF HEAT TREATMENT ON WEAR BEHAVIOR OF AlSi10Mg ALLOY FABRICATED BY CASTING

DÖKÜM İLE ÜRETİLEN AlSi10Mg ALAŞIMININ AŞINMA DAVRANIŞINA ISIL İŞLEMİN ETKİSİ

Halit ERCAN[1] **Kenan CAN**[2] **İbrahim Savaş DALMIŞ**[3]

https://doi.org/10.55071/ticaretfbd.1470743

Corresponding Author (Sorumlu Yazar)	*Received (Geliş Tarihi)*	*Revised (Revizyon Tarihi)*	*Accepted (Kabul Tarihi)*
idalmis@nku.edu.tr	*19.04.2024*	*15.10.2024*	*06.11.2024*

Abstract

The ease of processing aluminum due to its mechanical and chemical properties, along with various manufacturing methods, has increased its usage in the industry. This study involves tests conducted on the samples produced from EN AC-43000 (AlSi10Mg) aluminum casting material, which finds applications in machine manufacturing. The tests aimed to determine the mass loss and friction coefficients of the test specimens. Wear experiments were carried out according to ASTM G99 using a specialized test machine. The abrasive disc used in the wear machine has a surface hardness of 62 HRC and a surface roughness value (Ra) of 1,6 µm, and it is made of 1,2379-X155CrVMo12-1 cold work tool steel. Adhesive wear tests were conducted on the test specimens under loads of 14,7, 24,5, and 34,3 N. When the mass losses of the samples were examined, the wear rate decreased as the aging temperature increased up to 200 °C. On the other hand, it was observed that the wear rate increased at 220 °C, unlike aging at lower temperatures.

Keywords: Aging temperature, wear, adhesive wear, friction coefficient.

Öz

Alüminyumun mekanik ve kimyasal özelliklerinin yanısıra farklı imalat yöntemleri ile işlenebilirliğinin kolaylığı endüstride kullanımını arttırmıştır. Çalışmada makine imalatında da kullanım alanı bulan EN AC-43000 (AlSi10Mg) alüminyum döküm malzemeden üretilen numuneler ile yapılan testler ile test numunelerinin kütle kaybı ve sürtünme katsayıları saptanmıştır. Araştırmada aşınma deneyleri; ASTM G99'a göre imal edilmiş özel bir test makinesi ile gerçekleştirilmiştir. Aşınma makinesinde kullanılan aşındırıcı disk 62 HRC yüzey sertliği ve 1,6 µm yüzey pürüzlülük değerine (Ra) sahip; 1,2379-X155CrVMo12-1 soğuk iş takımı çeliğinden üretilmiştir. Çalışmada kullanılan test numunelerinin 14,7; 24,5 ve 34,3 N yük altında adhezif aşınma testleri gerçekleştirilmiştir. Numunelerin kütle kayıpları incelendiğinde, yaşlandırma sıcaklığı 200 °C'ye çıktıkça aşınma oranının azaldığı görüldü. Öte yandan, daha düşük sıcaklıklardaki yaşlandırmanın aksine, 220 C'de aşınma oranının arttığı gözlendi.

Anahtar Kelimeler: Yaşlandırma sıcaklığı, aşınma, adhezif aşınma, sürtünme katsayısı.

[*] *Bu yayın Halit ERCAN isimli öğrencinin Tekirdağ Namık Kemal Üniversitesi Fen Bilimleri Enstitüsü, Makine Mühendisliği Programındaki Yüksek Lisans tezinden üretilmiştir.*

[1] Tekirdağ Namık Kemal Üniversitesi, Çorlu Mühendislik Fakültesi, Makine Mühendisliği Bölümü, Tekirdağ, Türkiye. halittecann@gmail.com. Orcid.org/0009-0007-5454-2664.

[2] Tekirdağ Namık Kemal Üniversitesi, Çorlu Mühendislik Fakültesi, Makine Mühendisliği Bölümü, Tekirdağ, Türkiye. kcan@nku.edu.tr. Orcid.org/0000-0003-1770-1180.

[3] Tekirdağ Namık Kemal Üniversitesi, Çorlu Mühendislik Fakültesi, Makine Mühendisliği Bölümü, Tekirdağ, Türkiye. idalmis@nku.edu.tr. Orcid.org/0000-0002-4401-9155.

1. INTRODUCTION

The prevalent use of aluminum alloys in the industry is primarily due to their high specific strength, commendable corrosion resistance, and excellent thermal and electrical conductivity (Zang et al., 2023; Yan et al., 2020, Maji et al.,2020). Among aluminum alloys, Al-Si casting alloys, such as AlSi10Mg, play a crucial role in automotive and aerospace applications, particularly in components like combustion engines, clutches, pistons, pulleys, rockers, pivots, and liners (Gabor et al., 2022; Liu et al., 2021; Gite et al., 2023; Shakil et al., 2021; Shankar & Elango, 2017; Prasat et al., 2011; Dwivedi, 2006). Addition of silicon is known to enhance wear resistance in Al-Si alloys (Dwivedi, 2006; Kan et al., 2021).

Researchers have extensively investigated the mechanical and tribological behavior of Al-Si alloys. For instance, Prasat et al. (2011) studied the dry sliding wear and friction coefficient of AlSi10Mg-Fly ash–graphite hybrid composites, finding that sliding distance was the predominant factor influencing wear and friction coefficient. Senthilkumar et al. (2015) explored the dry sliding wear and friction behavior of AlSi10Mg alloy reinforced with rice husk ash, observing that the wear rate and friction coefficient were mainly influenced by the ratio of reinforcing particles, followed by applied load and sliding speed. Jiang et al. (2024) examined the effects of Mg-Gd master alloy addition on the microstructure and mechanical properties of Al-10Si aluminum alloy. As a result of the studies, they concluded that the addition of these alloys caused changes in the microstructure of the Al-10Si aluminum alloy and caused a significant increase in its mechanical properties. Kan et al. (2021) conducted a comprehensive investigation into the tribological properties of AlSi10Mg alloy fabricated by laser powder bed fusion. They subjected the alloy to dry sliding wear tests against both a bearing stainless steel and silicon carbide. The results indicated that the T6 heat treatment, either had no statistically significant effect or, in certain cases, adversely influenced the alloy's performance. Nirish and Rajendra (2022) investigated the wear and friction behavior of AlSi10Mg alloy produced through selective laser melting (SLM). They compared it to a conventionally cast Al6061 alloy. The researchers used a pin-on-disc machine to test the wear of the materials under different conditions. The findings unequivocally demonstrated that the SLM-AlSi10Mg alloy exhibited superior wear resistance and overall mechanical properties in comparison to as-cast Al6061. Gong et al. (2023), investigated the wear resistance of two aluminum alloys, Al-12Si and Al-2.5Fe, fabricated using laser powder bed fusion (LPBF). Their findings demonstrated that alloys produced via LPBF can exhibit exceptional wear resistance. They attributed this to the increased hardness resulting from the rapid cooling rate in the LPBF process, as well as the significant dispersion of fine secondary phases.

AlSi10Mg alloy, belonging to the hypoeutectic aluminum alloys group, typically contains 10 wt% Si and less than 0,45 wt% Mg (Gite et al., 2022; de Moura et al., 2022). This alloy is notable for not requiring preheating before and after casting (Senthilkumar et al., 2015). In this study, different aging temperatures and durations were applied to AlSi10Mg alloy after solution heat treatment at 540°C for 2 h and subsequent quenching. The precipitation hardening process yielded a coefficient of friction and adhesive wear values, determined by a test device conforming to ASTM G99.

2. MATERIAL AND METHOD

The material employed in the experimental studies is the AlSi10Mg casting alloy. The density of the test material is 2,66 g/cm^3. Test specimens prepared with dimensions of Ø10x20 mm were used in the experiment. The mass of the specimens was weighed before and after sliding wear by weighing machine with an accuracy of 0,0001 g after cleaning with alcohol.

All samples were solution heat treated at 540°C for 2 h and then quenched in water at room temperature. Then, artificial aging processes were carried out at temperatures of 160°C, 180°C, 200°C and 220°C (Table 1 and Figure 1). Girelli et al. (2018) applied precipitation hardening heat treatment to AlSi10Mg aluminum alloy in their study. In the experiments, the samples were solution heat treated at 480°C, 510°C and 540°C, and were artificially aged at 160°C for 4 h.

Table 1. Age Hardening Treatments

Specimen	Temperature (°C) (Tx)	Time (h)
1	160	4
2	180	4
3	200	4
4	220	4

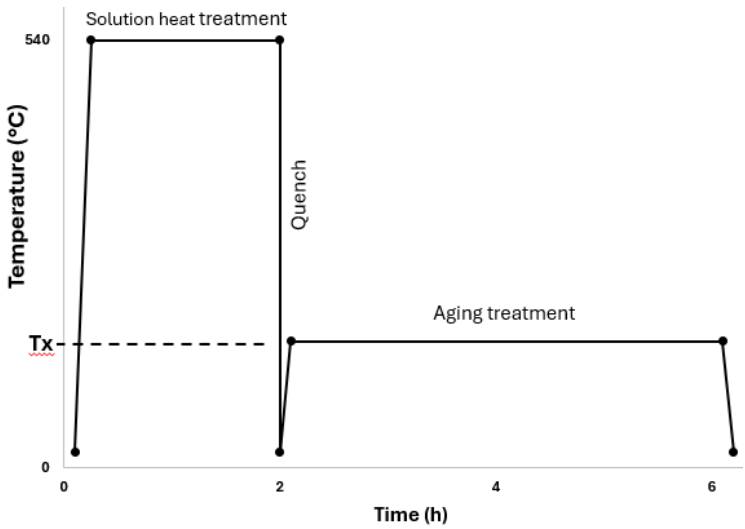

Figure 1. Diagrams Showing the Three Steps of Precipitation Hardening Applied to the 6 Test Specimens

A test machine designed and manufactured according to ASTM G-99 was used to evaluate the dry sliding wear and friction response of the specimen (Figure 2). Ø100x20 mm disc made of 1.2379-X155CrVMo12-1 cold work tool steel having a surface

hardness of 62 HRC and a surface roughness of 1,6 µm was used during the dry sliding wear test.

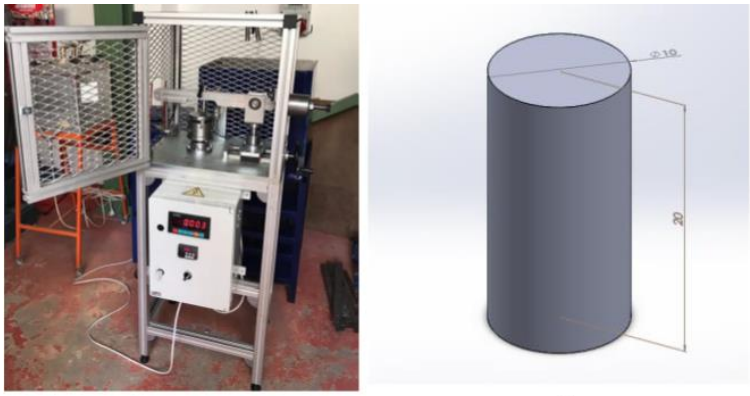

Figure 2. a) Adhesive Wear Testing Machine, b) Test Specimen Dimensions

Wear and friction characteristics of samples were evaluated at 1000 m sliding distances, 0,1 m/s sliding velocities, and 14,7 N, 24,5 N, and 34,3 N applied loads respectively. The tangential frictional force was obtained using the pin-on-disc machine during the sliding wear test. The coefficient of friction was calculated with the formula in Equation (1).

$$F_S = F_N.\mu \tag{1}$$

where F_S is the tangential frictional force, F_N is the normal force and μ is the coefficient of friction. The most used measurement method for calculating wear is the weight difference method. The Equations (2) and (3) used in the weight difference method are presented below (Soydaş, 2006).

$$Wa = \frac{\Delta G}{d.M.S}\ (mm^3/N.m) \tag{2}$$

where *Wa (mm³/N.m)* is the wear rate, *ΔG(mg)*, is the mass loss, *M* is the load (*N*), *S* is the wear distance (*m*), and *d* is the density (*gr/cm³*).

Wear resistance (W_r) is defined as the inverse of the wear rate and is shown in Equation (3).

$$W_r = \frac{1}{W_a}\ (N.m/mm^3) \tag{3}$$

The wear surfaces of the samples were examined with an Optika B-500 MET optical microscope. To determine the hardness of samples, a microhardness test was performed with an HV hardness scale under 100 g loads by a Microbul 1000-DN test device. Microhardness measurements were carried out by taking the average of a total of 5 measurement values taken from each sample. (Can et al., 2022)

3. RESULT AND DISCUSSION

Mass losses of the specimens and microhardness values are given in Table 2. Figure 3 also shows the mass losses of specimens depending on the applied loads. Averages of the F values and coefficient of friction (CoF) are given in Table 3.

Table 2. Age Hardening Treatments

Specimen	Applied Load (N)			Total mass loss (mg)	Hardness
	14,7 N	24,5 N	34,3 N		$HV_{0,1}$
	Mass loss (mg)	Mass loss (mg)	Mass loss (mg)		
1	5,3	7,8	10,2	23,3	79,3
2	5,4	7,6	10	23	85,16
3	4,6	7,2	9,8	21,6	133,14
4	6,3	8,5	11	25,8	68,8

It has been determined that the coefficient of friction "μ" values obtained as a result of the wear tests for each sample with different weights have approximately the same values even if the weight increases. The highest coefficient of friction value is seen in the 4th sample with an average value of 0,883, and the lowest coefficient of friction value is seen in the 3rd specimen with an average of 0,785 (Figure 4).

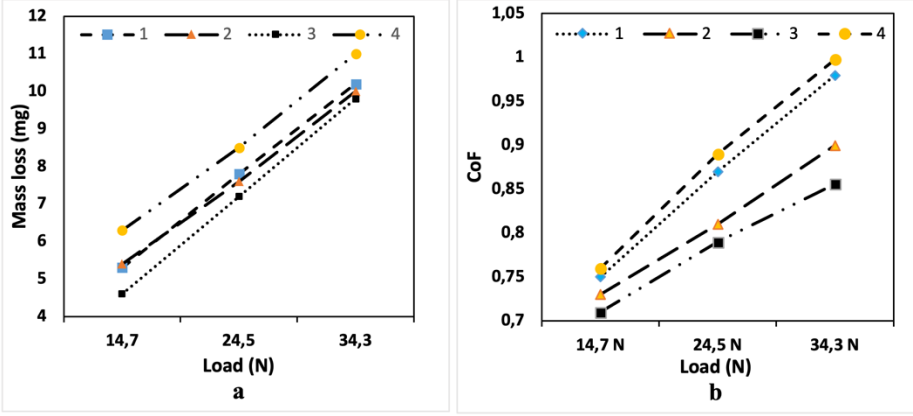

Figure 3. Variation in (a) Mass Loss of Specimens and
(b) Average Friction Coefficient of Specimens Under Different Loads

Table 3. Values of Average F and Coefficient of Friction (COF)

Specimen	Applied Load (N)						Average CoF
	14,7 N		24,5 N		34,3 N		
	F_{Av}	CoF	F_{Av}	CoF	F_{Av}	CoF	
1	11,03	0,75	21,32	0,87	33,61	0,98	0,867
2	10,73	0,73	19,85	0,81	30,87	0,9	0,813
3	10,44	0,71	19,36	0,79	29,36	0,856	0,785
4	11,17	0,76	21,81	0,89	34,23	0,998	0,883

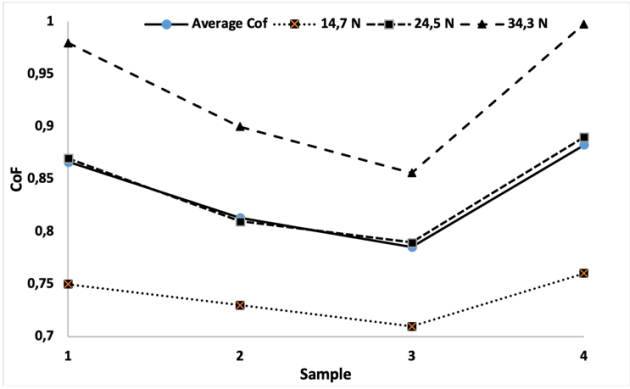

Figure 4. Average CoF Values of All Specimens

When Figure 5 is examined, mass losses depending on the hardness of the samples can be seen. The graph shows us the relationship between hardness and wear, and as hardness increases, wear decreases accordingly. Beder et al. (2023) also stated that hardness affects wear.

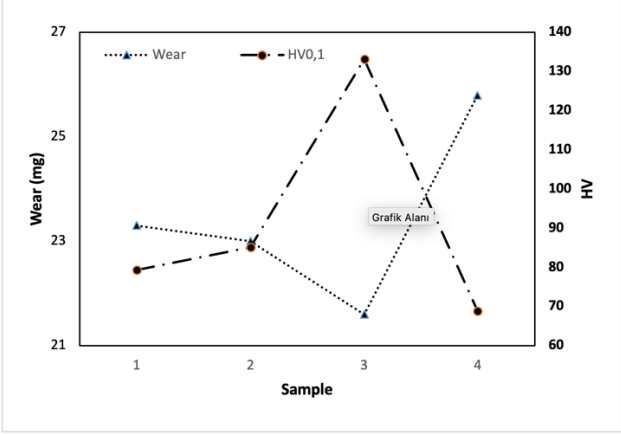

Figure 5. Total Mass Loss Versus Hardness of Samples

Average wear rates and average wear resistances of the samples are presented in Table 4 and Table 5. Figure 6 and Figure 7 obtained from these tables show us the relationship between the CoFs and wear rates of the samples and the relationship between hardness and wear resistance, respectively.

Table 4. Values of Average Wear Rate

Specimen	Applied Load (N)			Average wear rate ($mm^3/N.m$) $x10^{-4}$
	14,7 N	24,5 N	34,3 N	
	Wear rate ($mm^3/N.m$) $x10^{-4}$	Wear rate ($mm^3/N.m$) $x10^{-4}$	Wear rate ($mm^3/N.m$) $x10^{-4}$	
1	1,36	1,20	1,09	1,21
2	1,38	1,17	1,06	1,20
3	1,18	1,10	1,04	1,11
4	1,61	1,30	1,17	1,36

Table 5. Values of Average Wear Resistance

Specimen	Applied Load (N)			Average wear resistance ($mm^3/N.m)^{-1}x10^4$
	14,7 N	24,5 N	34,3 N	
	Wear resistance ($mm^3/N.m)^{-1}x10^4$	Wear resistance ($mm^3/N.m)^{-1}x10^4$	Wear resistance ($mm^3/N.m)^{-1}x10^4$	
1	0,74	0,84	0,92	0,83
2	0,72	0,86	0,94	0,84
3	0,85	0,91	0,96	0,90
4	0,62	0,77	0,85	0,75

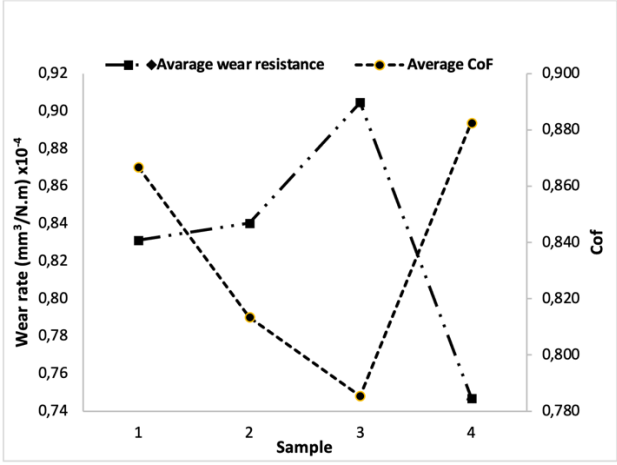

Figure 6. The Wear Rate and Average Friction Coefficient at the Samples

A comparison of the average steady-state coefficient of friction (CoF) values for the samples is shown in Fig. 6. The CoF values for all samples ranged between 0,80 and 0,89, with minimal variation, except for a slightly higher value observed for sample S4. These CoF values are consistent with the range typically seen in aluminum alloys under dry sliding conditions, which generally spans from 0,4 to 0,9, depending on the specific test conditions and alloy used (Straffelini, 2015). Therefore, it can be concluded that the heat treatment conditions and the resulting differences in microstructure and hardness for the AlSi10Mg alloy (as seen in Fig. 6) do not significantly impact the CoF, as noted in previous studies (Straffelini, 2015; Ren et al., 2023).

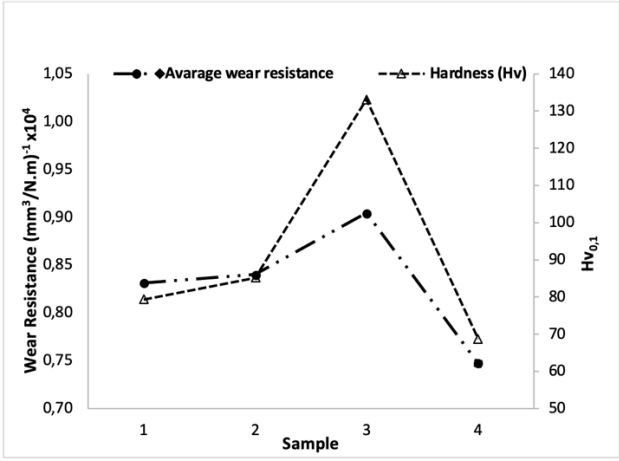

Figure 7. The Average Wear Resistance and Hardness of the Samples

After conducting the wear tests, the worn surfaces of the samples were observed using an optical microscope. It was identified that there are variations in elevation between the dark and bright areas, attributed to adhesive fractures. Furthermore, the lines

observed in the sliding direction within the bright areas were identified as abrasive wear lines, formed by the adhesive wear debris that accumulated on the surface of the abrasive disc.

Numerous studies on wear mechanisms validate the link between adhesive and abrasive wear, as well as the subsequent formation of wear lines during sliding. Adhesive wear typically begins when surfaces come into contact, leading to material transfer. Over time, this transferred material becomes embedded between the surfaces, contributing to the formation of abrasive wear patterns, often observed as grooves or lines parallel to the sliding direction (Chawla & Chawla, 2013). The presence of wear debris on the abrasive surface further intensifies the wear process, resulting in visible scratches, especially in the bright areas, where the material becomes more polished due to prolonged friction (Straffelini, 2015).

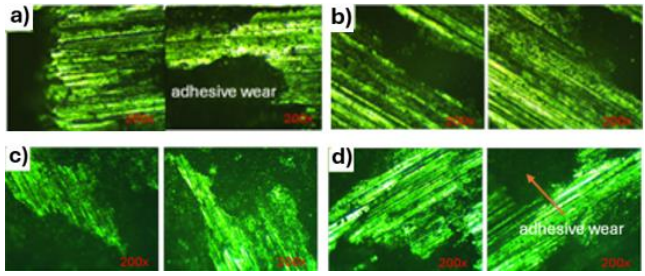

Figure 8. Wear Surface of Specimens, a) S1, b) S2, c) S3, d) S4 (200x Magnification)

The differences in CoF trends in Fig. 6 can be explained by the stability of the transfer layers formed at the contact interface during wear tests. The second hard phase, composed of Si particles, plays a significant role in this. These particles can cause localized fracture phenomena, thereby disrupting the formation of a protective transfer layer on the worn surface. This is evident in Fig. 8(a–d), where thick transfer layers formed on the counter material surfaces due to severe adhesive wear of the AlSi10Mg disk (Fig. 9(e–d)). The presence and stability of these layers correlate with wear depth (WD).

From the observations, the average WD values suggest that WD is lower for sample S3 compared to S1, and in general, WD increases as hardness decreases (as shown in Fig. 7). This trend is linked to the microstructural differences in the alloy, particularly the distribution of silica grains and the α phase, which are crucial for determining mechanical properties.

Moreover, aging heat treatments induce the nucleation of θ particles within the α grains, contributing to the alloy's mechanical behavior. Although these θ particles are too small to detect optically, their influence can be indirectly observed via hardness tests. The microstructural images in Fig. 9 also show that the silica grains are partially reduced after aging, further influencing mechanical performance (Beder et al., 2023).

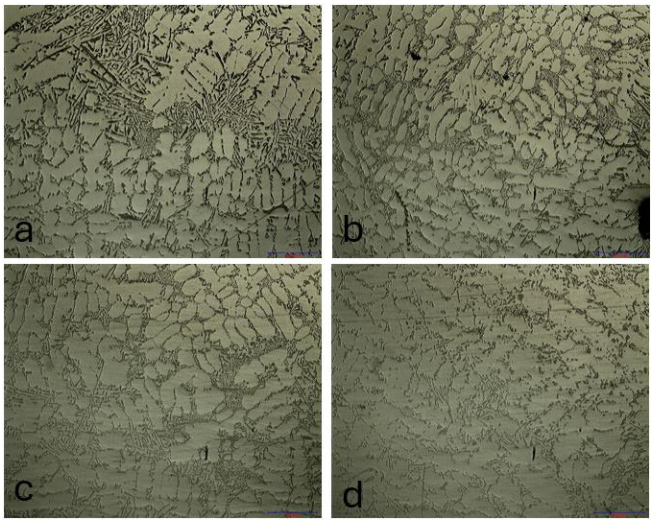

Figure 9. Light Microscopy (LM) Image of the Microstructure of Hypoeutectic AlSi10Mg Alloy
a) S1, b) S2, c) S3, d) S4 (mass loss are 3<2<1<4, respectively) (X250)

The decline in mechanical properties of aluminum alloys when aging temperatures exceed 200°C is primarily attributed to overaging. During this process, the microstructure of the alloy coarsens, weakening the strengthening effect achieved through the precipitation of fine particles. Up to 200°C, precipitates like the β″ phase in Al-Mg-Si alloys form and are finely dispersed, which impedes dislocation motion, thereby strengthening the material via precipitation hardening (Ren et al., 2023; Chang et al., 2024).

However, when the aging temperature surpasses 200°C, these precipitates begin to grow and coarsen. The larger precipitates are less effective at blocking dislocations, resulting in decreased mechanical strength and hardness. At 220°C and higher, this coarsening becomes more pronounced, making the alloy softer and more susceptible to wear (Chang et al., 2024). Additionally, higher temperatures can lead to the formation of secondary or unstable phases, which further degrade the alloy's resistance to mechanical stress.

In samples aged at higher temperatures, such as S4, the dissolved silicon (as seen in Fig. 9) increases, indicating a need to examine the long-term stability of mechanical properties in as-built structures. Up to 200°C, precipitates survive and grow, filling the cell centers and contributing to higher hardness values through both precipitation hardening and Hall-Petch strengthening mechanisms, as observed in Fig. 6. The presence of Mg_2Si particles also contributes to this enhanced hardness, although the influence of dislocations becomes limited at higher temperatures (Ren et al., 2023).

4. CONCLUSION

In the study, the effects of different aging temperatures applied to test samples produced from EN AC-43000 (AlSi10Mg) aluminum casting material were examined. It was observed that although sample number 1 suffered more mass loss than sample number 2 at 24,5 and 34,3 N loads, it showed a lower mass loss than sample number 2 under 14,7 N load, unlike the other loads. It is thought that the reason for this is that the wear mechanism changes from adhesive wear to abrasive wear. When Figure 3b is examined, under 14,7 N load, the CoF graph of sample 1 tends to decrease, while the CoF graph of sample 2 tends to increase, and this strengthens our opinion that the wear mechanism has changed. Considering the result of the wear values obtained from the samples, the mass loss of sample 4 is higher than the other samples. It has been observed that as a result of adhesive wear, the fragments pulled off from the samples adhered to the abrasive disc surface, resulting in abrasive wear and serious scratches. Considering the total mass losses, the samples with the least mass loss are 3<2<1<4, respectively. In the tests performed, the CoF value was low in samples 2 and 3. The wear to which these samples are exposed is considered to be mostly abrasive wear. It was seen that the CoF value was high in numbers 1 and 4, and when the microstructures were examined, it was concluded that the wear type here was adhesive wear. Finally, when the mass losses of the samples were examined, it can be said that the increase in aging temperature increased the wear resistance but after 220 °C depending on the hardness loss wear resistance decreased.

Authorship Contributions
The authors confirm that they equally contributed to this paper.

Acknowledgment
The test rig manufacturing processes used in the study were supported by Dogan Mekatronik.

Conflict of Interest
The authors declare that there is no conflict of interest.

Statement of Research and Publication Ethics
Research and publication ethics were observed in the study.

REFERENCES

Beder, M., Akçay, S. B., Varol, T., & Çuvalcı, H. (2024). The Effect of Heat Treatment on the Mechanical Properties and Oxidation Resistance of AlSi10Mg Alloy. *Arabian Journal for Science and Engineering,* 1-12.

Can, K., Dalmış, F., & Dalmış, İ. (2022). Design and Implementation of PLC Based Special Purpose Machine for Surface Coating. *Avrupa Bilim ve Teknoloji Dergisi,* (33), 338-343.

Chang, Z., Liu, L., Sui, Z., Yan, X., Li, Y., Zhang, Y., ... & Yang, M. (2024). Effect of Aging Temperature on Pitting Corrosion of AA6063 Aluminum Alloy. *Metals and Materials International,* 30(6), 1556-1570.

Chawla, N., Chawla, K.K. (2013). *Wear and Corrosion. In: Metal Matrix Composites*. Springer, New York, NY. https://doi.org/10.1007/978-1-4614-9548-2_10

de Moura, D. A., de Gouveia, G. L., Gomes, L. F., & Spinelli, J. E. (2022). Understanding the effect of Ni content on microstructures and tensile properties of AlSi10Mg alloy samples under a variety of solidification rates. *Journal of Alloys and Compounds,* 924, 166496.

Dwivedi, D. K. (2006). Wear behaviour of cast hypereutectic aluminium silicon alloys. *Materials & design,* 27(7), 610-616.

Gabor, R., Prymus, T., Cvrček, L., Nehasil, V., Hlinka, J., Buřil, M., ... & Seidlerová, J. (2022). Final surface modification for better wear resistance of ceramic coating on cast AlSi10Mg alloy. *Ceramics International*, 48(24), 37433-37447.

Gite, R. E., & Wakchaure, V. D. (2023). A review on process parameters, microstructure and mechanical properties of additively manufactured AlSi10Mg alloy. *Materials Today: Proceedings,* 72, 966-986.

Gong, S., Takata, N., Kobashi, M., & Shin, S. E. (2023). Wear properties of aluminum alloys fabricated by laser powder bed fusion. *Tribology International,* 187, 108769.

Jiang, B., Jiang, B., Yang, W., Wang, Y., Xu, H., Hu, M., & Guo, Y. (2024). Efficient modification eutectic Si of Al-10Si alloy with Mg-Gd master alloy addition. *Materials Letters,* 136071.

Kan, W. H., Huang, S., Man, Z., Yang, L., Huang, A., Chang, L., ... & Proust, G. (2021). Effect of T6 treatment on additively-manufactured AlSi10Mg sliding against ceramic and steel. *Wear,* 482, 203961.

Liu, C., Wang, Q., Cao, X., Cha, L., Ye, R., & Ramachandran, C. S. (2021). Significance of plasma electrolytic oxidation treatment on corrosion and sliding wear performances of selective laser melted AlSi10Mg alloy. *Materials Characterization,* 181, 111479.

Maji, P., Ghosh, S. K., Nath, R. K., & Karmakar, R. (2020). Microstructural, mechanical and wear characteristics of aluminum matrix composites fabricated by friction stir processing. *Journal of the Brazilian Society of Mechanical Sciences and Engineering,* 42, 1-24.

Nirish, M., & Rajendra, R. (2022). Optimization Process Parameter on Wear Characterization of Al6061 and AlSi10Mg Alloy Manufactured by Selective Laser Melting. International *Journal of 3D Printing and Additive Manufacturing,* 2(1), 1-10.

Prasat, V., Subramanian, R., Radhika, N., & Anandavel, B. (2011). Dry sliding wear and friction studies on AlSi 10 Mg-fly ash-graphite hybrid metal matrix composites using Taguchi method. *Tribology- Materials, Surfaces & Interfaces,* 5(2), 72-81.

Ren, J., Hong, Z., Zhou, Q., Xu, X., & Yin, S. (2023). Effect of Aging Treatment Temperature on Microstructure and Properties of Al-Si-Mg Cast Aluminum Alloy. *Journal of Materials Engineering and Performance,* 1-9.

Senthilkumar, M., Saravanan, S. D., & Shankar, S. (2015). Dry sliding wear and friction behavior of aluminum–rice husk ash composite using Taguchi's technique. *Journal of composite materials,* 49(18), 2241-2250.

Shakil, S. I., Hadadzadeh, A., Pirgazi, H., Mohammadi, M., & Haghshenas, M. (2021). Indentation-derived creep response of cast and laser powder bed fused AlSi10Mg alloy: Air temperature. *Micron,* 150, 103145.

Shankar, S., & Elango, S. (2017). Dry sliding wear behavior of palmyra shell ash–reinforced aluminum matrix (AlSi10Mg) composites. *Tribology Transactions,* 60(3), 469-478.

Soydaş, S. (2006). *Üniversal aşınma test cihazı tasarımı ve imalatı* [Master's thesis]. Kocaeli Üniversitesi Fen Bilimleri Enstitüsü, Kocaeli.

Straffelini, G. (2015). *Wear Mechanisms. In: Friction and Wear.* Springer Tracts in Mechanical Engineering. Springer, Cham. https://doi.org/10.1007/978-3-319-05894-8_4

Wahlström, J., Lyu, Y., Matjeka, V., & Söderberg, A. (2017). A pin-on-disc tribometer study of disc brake contact pairs with respect to wear and airborne particle emissions. *Wear,* 384, 124-130.

Yan, Q., Song, B., & Shi, Y. (2020). Comparative study of performance comparison of AlSi10Mg alloy prepared by selective laser melting and casting. *Journal of Materials Science & Technology,* 41, 199-208.

Zhang, P., Liu, J., Gao, Y., Liu, Z., & Mai, Q. (2023). Effect of heat treatment process on the micro machinability of 7075 aluminum alloy. *Vacuum,* 207, 111574.